

ROLE OF FLUCTUATIONS IN FLUID MECHANICS AND DENDRITIC SOLIDIFICATION

H. Eugene STANLEY

Center for Polymer Studies and Department of Physics, Boston University, Boston, MA 02215, USA

Many recent advances have occurred in our understanding of the role of fluctuations in fluid mechanics and dendritic solidification. Our purpose here is to present a review of some of these. We shall argue that if one understands completely the simple diffusion-limited aggregation (DLA) model or the closely related dielectric breakdown model (DBM), one understands the role of fluctuations in a range of fluid mechanical systems, as well as in dendritic solidification. The detailed descriptions of some such systems requires suitably chosen variants, such as DBM with anisotropy and noise reduction.

1. Introduction

The theme I shall develop is that recent work on relatively simple *non-deterministic* models has some utility for describing experimentally observed phenomena in fluid mechanics and dendritic growth. I shall first make the case that we can approach these experimental subjects of classic difficulty with the same spirit that has been used in recent years to approach problems associated with phase transitions and critical phenomena. This approach is to carefully choose a microscopic model system that captures the essential physics underlying the phenomena at hand, and then study this model until we understand ‘how the model works’. Then we reconsider the phenomena at hand, to see if an understanding of the model leads to an understanding of the phenomena. Sometimes the original model is not enough, and a variant is needed, and we shall see that this is the case here also. Fortunately, however, we shall see that the same underlying physics is common to the model and its variants.

2. The Ising model and its ‘variants’

We begin, then, with the classic Ising model [1–2]. Over 1000 papers have been published on this model, but only since 1977 have we known that if one understands the Ising model thoroughly, one understands the essential physics

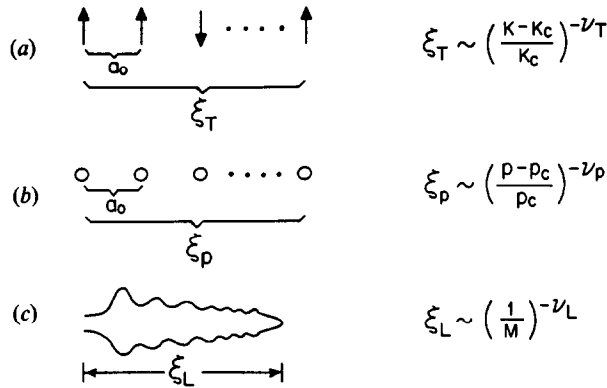


Fig. 1. Schematic illustration of the analogy between (a) the Ising model, which has fluctuations in spin orientation on all length scales from the microscopic scale of the lattice constant a_0 up to the macroscopic scale of the thermal correlation length ξ_T , (b) percolation, which has fluctuations in characteristic size of clusters on all length scales from a_0 up to the diameter of the largest cluster – the pair connectedness length ξ_p , and (c) the DLA/DBM problem, whose clusters have fluctuations on all length scales from the microscopic length $d_0 = \gamma/L$ (γ is the surface tension and L the latent heat) up to the diameter of the cluster ξ_L . Also shown, on the right side, is the analogy between the scaling behavior of the three length scales ξ_T , ξ_p , and ξ_L .

of many materials, since they are simply variants of the Ising model. For example, a large number of systems are related to special cases of the n -vector model, which in turn is a simple Ising model in which the spin variable s has not one component but rather n separate components s_j : $s \equiv (s_1, s_2, \dots, s_n)$.

The Ising model solves the puzzle of how it is that nearest-neighbor interactions of microscopic length scale 1 \AA ‘propagate’ their effect cooperatively to give rise to a correlation length ξ_T of macroscopic length scale near the critical point (fig. 1a). In fact, ξ_T increases without limit as the coupling $K \equiv J/kT$ increases to a critical value $K_c \equiv J/kT_c$,

$$\xi_T \sim A \left(\frac{K - K_c}{K_c} \right)^{-\nu_T}. \tag{1a}$$

The ‘amplitude’ A has a numerical value of the order of the lattice constant a_0 . A snapshot of an Ising system shows that there are fluctuations on all length scales from a_0 ($\cong 1 \text{ \AA}$) to ξ_T (which can be 10^2 – 10^4 \AA in a typical experiment).

3. Random-site percolation on a lattice, and its variants

In percolation, one randomly occupies a fraction p of the sites of a d -dimensional lattice (the case $d = 1$ is shown schematically in fig. 1b). Again,

phenomena occurring on the local 1 \AA scale of a lattice constant are ‘amplified’ near the percolation threshold $p = p_c$ to a macroscopic length ξ_p .

Here, p plays the role of the coupling constant K of the Ising model. When p is small, the characteristic length scale is comparable to 1 \AA . However, when p approaches p_c , there occur phenomena on all scales ranging from a_0 to ξ_p , where ξ_p increases without limit as $p \rightarrow p_c$,

$$\xi_p \sim A \left(\frac{p - p_c}{p_c} \right)^{-\nu_p}. \quad (1b)$$

Again, the amplitude A is roughly a lattice constant ($\sim 1 \text{ \AA}$).

Each phenomenon of thermal critical phenomena has a corresponding analog in percolation, so that the percolation problem is sometimes called a geometric or *connectivity* critical phenomenon. Any connectivity problem can be understood by starting with pure random percolation and then adding interactions, or whatever. Thus, e.g., we understand why the critical exponents describing the divergence to infinity of various geometrical quantities (such as ξ_p) are the same regardless of whether the elements interact or are non-interacting [3–4]. Similarly, the same connectivity exponents are found regardless of whether the elements are constrained to the sites of a lattice or are free to be anywhere in a continuum [4–6].

4. The Laplace equation and its variants

Just as variations in the Ising and percolation problems were found to be sufficient to describe a rich range of thermal and geometric critical phenomena, so we have found that variants of the original Laplace equation are useful in describing puzzling patterns in fluid mechanics, dendritic growth, and various breakdown phenomena (see table I).

In the Ising model, we place a spin on each pixel (site) of a lattice. In percolation we allow each pixel to be occupied or empty. In fluid mechanics, we assign a number – call it ϕ – to each pixel. We might think of ϕ as being the pressure or chemical potential at this region of space.

The spins in an Ising model interact with their neighbors. Hence, the state of one Ising pixel depends on the state of all the other pixels in the system – up to a length scale given by the thermal correlation length ξ_T . The ‘global’ correlation between distant pixels in an Ising simulation arises from the fact that neighboring pixels at i and j have a ‘local’ exchange interaction J_{ij} . Similarly, the correlation in connectivity between distant pixels in the percolation problem arises from the ‘propagation’ of local connectivity between

neighboring pixels. In fluid mechanics, the pressure on each pixel is correlated with the pressure at every other pixel because the pressure obeys the Laplace equation.

One can calculate an equilibrium Ising configuration by ‘passing through the system with a computer’ and flipping each spin with a probability related to the Boltzmann factor. Similarly, one can calculate the pressure at each pixel by ‘passing through the system’ and re-adjusting the pressure on each pixel in accord with the Laplace equation. If we were to arbitrarily flip the configuration of a single pixel in the Ising problem (from +1 to -1), we would significantly influence the equilibrium configuration of the system out to a length scale on the order of ξ_T . Similarly, if we were to arbitrarily impose a given pressure on a single point of a system obeying the Laplace equation, we would drastically change the resulting pattern out to a length scale that we shall call ξ_L .

Does ξ_L obey a ‘scaling form’ analogous to eqs. (1a) and (1b) obeyed by the functions ξ_T and ξ_p for the Ising model and percolation? We believe that the answer to this question is ‘yes’, although our ideas on this subject remain somewhat tentative and subject to revision.

The best way to see the fluctuations inherent in structures grown according to the Laplace equation is to first introduce some specific models. There are two models that were at once thought to be fully equivalent, although it is now recognized that the actual patterns produced by each have a different ‘susceptibility to lattice anisotropy’ [7–8]. The first of these models is diffusion limited aggregation (DLA) [1]. Here, one releases a random walker from a large circle surrounding a seed particle placed at the origin. When the random walker

Table I

A ‘Rosetta stone’ connecting the physics underlying (a) an electrical problem (dielectric breakdown), (b) a fluid mechanics problem (viscous fingering), and (c) a diffusion problem (dendritic solidification).

(a) electrical	(b) fluid mechanics	(c) dendritic solidification
Electrostatic potential: $\phi(r, t)$	Pressure: $P(r, t)$	Concentration: $c(r, t)$
Electric field: $E \propto -\nabla\phi(r, t)$	Velocity: $v \propto -\nabla P(r, t)$	Growth rate: $v \propto -\nabla c(r, t)$
Conservation: $\nabla \cdot E = 0$	$\nabla \cdot v = 0$	$\nabla \cdot v = 0$
Laplace equation: $\nabla^2\phi = 0$	$\nabla^2 P = 0$	$\nabla^2 c = 0$

touches a perimeter site of the seed, it ‘sticks’ (i.e., the perimeter site becomes a cluster site), and we have a cluster of mass $M = 2$. A second random walker is then released. This process continues until a large cluster is formed.

In both thermal critical phenomena (or percolation) the length L introduced when we have a finite system size scales the same as the correlation lengths ξ_T (or ξ_p). Hence, for DLA we expect that there will be fluctuations on length scales up to ξ_L , where ξ_L itself increases with the cluster mass according to

$$\xi_L \sim A \left(\frac{1}{M} \right)^{-\nu_L} \quad \left[d_f \equiv \frac{1}{\nu_L} = \text{fractal dimension} \right]. \quad (1c)$$

Here, the amplitude A is again of the order of 1 \AA . Note that eq. (1c) is analogous to (1a) and (1b) if we think of $M \rightarrow \infty$ as being analogous to $K \rightarrow K_c$. Note also that $\nu_L = 1/d_f$ plays the role of the critical exponents ν_T and ν_p of (1a) and (1b). Suppose one tests this idea, qualitatively, by examining the largest DLA clusters in detail. One finds that indeed there are fluctuations in mass on length scales less than, say, the width W of the side branches. If one makes a log–log plot of W against mass M , one finds the same slope $1/d_f$ that one finds when one plots the diameter against M^2 .

5. Evidence for similarity of viscous fingering patterns and Laplace equation (DLA/DBM) patterns

In the remainder of this talk, I shall describe in some detail the sorts of results we obtain from variants of the Laplace equation. First, it is necessary to describe the simplest system that produces patterns resembling interesting objects found in nature. Consider, e.g., the classic Saffman–Taylor viscous fingering problem. Here, one injects a low-viscosity fluid into a medium filled with high-viscosity fluid. In the limit that the viscosity ratio between the high- and low-viscosity fluids can be taken to be zero, we can assume that the pressure everywhere inside the low-viscosity fluid is a constant: $P(i) = 1$ for $i \in [\text{cluster of pixels occupied by low-viscosity fluid}]$. The pressure everywhere else in the system will have a value given by the solution of the Laplace equation, (1c). This problem is modelled by the dielectric-breakdown model or DBM [10] or diffusion-limited aggregation model or DLA [11]. These two models have in common that both are solutions to the Laplace equation for the case in which the pressure is zero at infinity and $P = 1$ on an object called the cluster.

Daccord has made accurate measurements on the fractal dimension of viscous fingers in both lateral [12] and radial [13] geometries (fig. 2). He

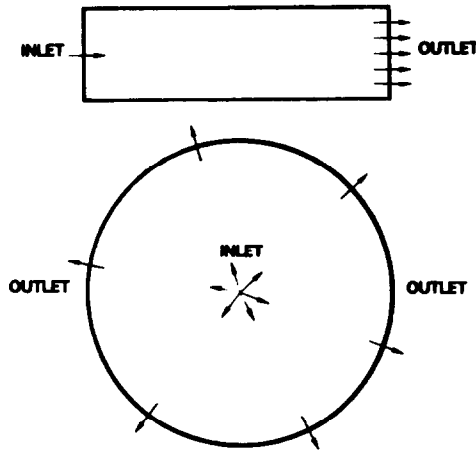


Fig. 2. Schematic illustration of the lateral and radial Hele–Shaw cells. Shown are top views. The spacing between the plates is typically 1 mm or less (from Daccord et al. [13]).

reduced the length scale normally imposed by surface tension by using liquids with zero interfacial tension – the two fluids were water and viscous aqueous solution of polysaccharide (fig. 3). He found that the resulting patterns are indeed fractal, with a fractal dimension identical to that of DLA/DBM (fig. 4). Måløy et al. [14] found analogous behavior where the cell itself introduced the randomness: he accomplished this by placing glass beads inside the cell at random. Chen and Wilkinson [15] imposed the randomness by studying viscous fingering inside a network of glass tubes whose diameter L was randomly chosen from a probability distribution $\pi(L)$.

Not only is the fractal dimension the same for the fluid-mechanics problem and for the Laplace patterns, but *so also are the multifractal properties the same*. Multifractals arise when one defines some quantity on all the pixel sites. Perhaps the simplest example is that of a charged needle: if we assign to every pixel a number equal to the electric field, then the set $\{E_i\}$ of field values for the perimeter sites of the needle form a multifractal set. The distribution $n(E)$ giving the number of perimeter pixels with electric field E is characterized, like all distribution functions, by its moments

$$Z(q) = \sum_E n(E) E^q. \quad (2)$$

As might be anticipated for a self-similar system, these moments scale with the mass M (or with the diameter L)

$$Z(q) \sim M^{\sigma(q)} \sim L^{-\tau(q)}. \quad (3a)$$

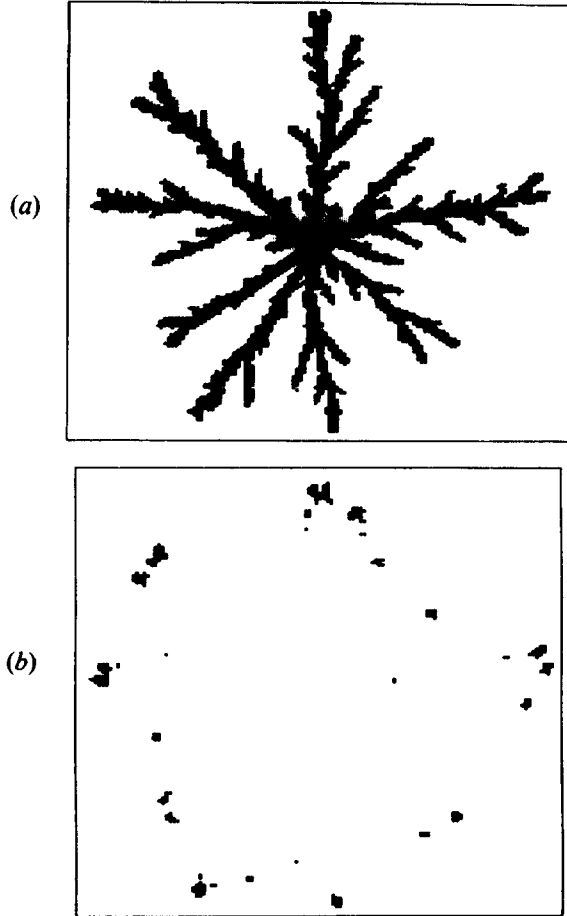


Fig. 3. The growth region of a radial viscous finger, a typical experimental pattern for which DLA is the appropriate model. The finger at time $t = t_0$ is shown in (a), while (b) displays the difference between the pattern at $t = t + \Delta t$ and $t = t$, obtained experimentally by simply subtracting the images of the same finger photographed at slightly different times (after Daccord et al. [13]).

Since $M \sim L^{d_f}$, the exponents σ and τ are related by the fractal dimension d_f ,

$$\sigma = \frac{\tau}{d_f}. \quad (3b)$$

For thermal and geometric critical phenomena, exponents analogous to the $\sigma(q)$ and $\tau(q)$ can be defined by considering a large $L \times L$ system at the critical point ($K = K_c$) (or $p = p_c$). One finds that the ratio of two successive exponents is a constant 'gap', so that there is no new information obtained by studying higher moments of the distribution. Connected with this simplicity is the fact that there is only one independent exponent in finite-size scaling at the

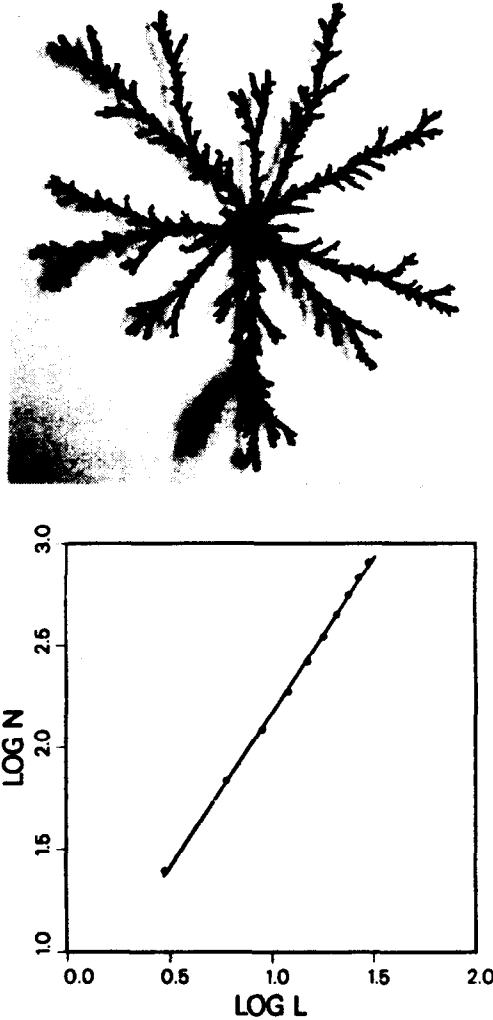


Fig. 4. Analysis of the fractal dimension typical of a radial viscous finger by the sandbox method (N is the number of occupied pixels in a $L \times L$ sandbox whose center is on an occupied pixel). The slope of the straight line shown is $d_f = 1.70 \pm 0.05$, while for DLA d_f is believed to be about 1.71 (from Daccord et al. [13]).

critical point (a second exponent arises if we wish to relate quantities that describe the approach to the critical point).

In the case of the moments Z_q , there is an infinite hierarchy of exponents in the sense that the ratio $\tau(q+1)/\tau(q)$ depends on q ,

$$\frac{\tau(q+1)}{\tau(q)} = D(q). \quad (4)$$

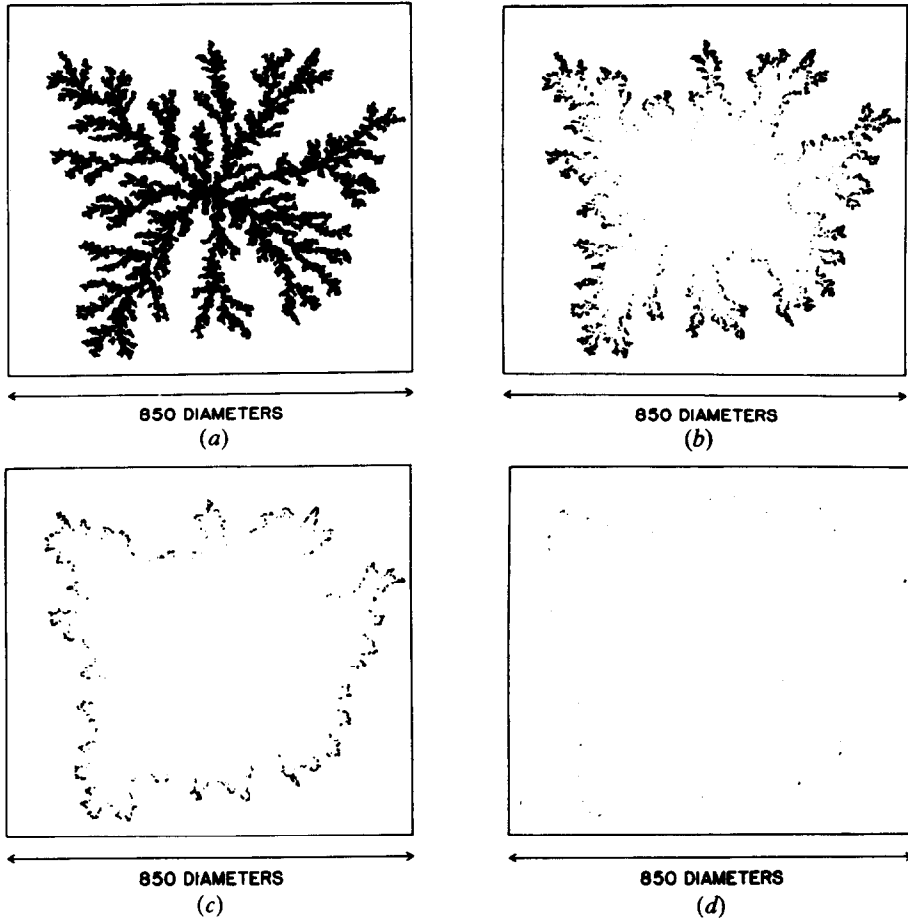


Fig. 5. This figure illustrates the harmonic measure for a 50 000 particle off-lattice two-dimensional aggregate. Fig. 5a shows the cluster. Fig. 5b shows all 6803 perimeter sites which have been contacted by at least one of 10^6 random walkers (following off-lattice trajectories). Fig. 5c shows all of those perimeter sites which have been contacted 50 or more times and Fig. 5d shows those sites which have been contacted 2500 or more times. The maximum number of contacts for any perimeter site was 8197 so that $p_{\max} = 8.2 \times 10^{-3}$ (after Meakin et al. [19]).

For the case of a long thin needle, the exponent $D(q)$ sticks at the value $\frac{3}{2}$ for small q , but for q above a critical value $q = q_c$, $D(q)$ becomes 'unstuck' and varies continuously with q .

The same considerations apply to the fluid-mechanics problem. Here, the analog of the electric field $E \propto \nabla V$ is the growth probability $p_i \propto \nabla P$, where the index i runs over all perimeter sites i . Thus, p_i is the probability that site i is the next to be added to the cluster. If we think of random walkers (fig. 5), then p_i is the hit probability (the probability that site i is the next to be hit by a

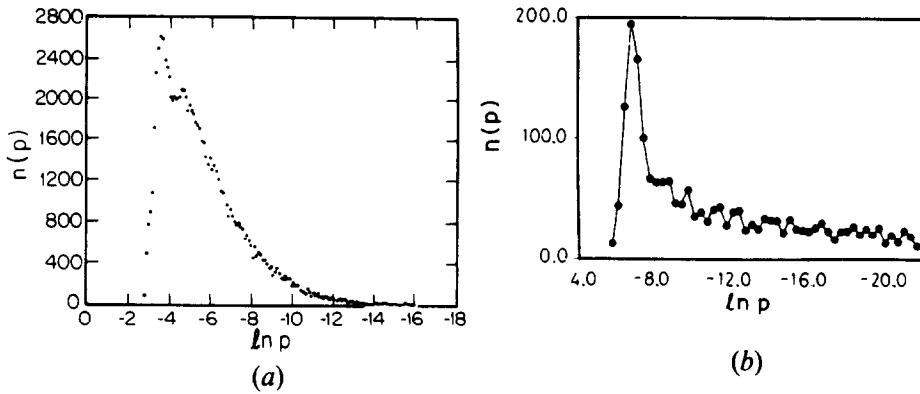


Fig. 6. Comparison between the distribution functions $n(p)$ for (a) simulated and (b) 'experimental' viscous fingering patterns. Here $n(p) dp$ is the number of perimeter sites with growth probabilities in the range $[p, p + dp]$. The simulated patterns and their growth probabilities were obtained using the dielectric breakdown model. The growth probabilities for the experimental patterns were obtained by numerically solving the Laplace equation in the vicinity of a digitized representation of the pattern with absorbing boundary conditions on the sites occupied by the pattern. Similar results were obtained for large α (corresponding to the 'tips') by directly subtracting two successive experimental patterns (after Amitrano et al. [40] and Nittmann et al. [41]).

random walker). Clearly, the set p_i play a vital role in determining the dynamics of growth, since if we know all the p_i for every perimeter site i at a given time t , then we can predict (in a statistical sense) the state of the system at time $t + 1$.

Recently, considerable attention has focussed on the question of how a DLA aggregate grows. Such growth phenomena are *completely* characterized by assigning to each perimeter site i the number p_i , the probability that site i is the next to grow.

Theoretical evidence has been advanced recently to suggest that the numbers p_i form a multifractal set: this set cannot be characterized by a single exponent (as in the case of the DLA aggregate itself), but rather an infinite hierarchy of exponents is required. The physical basis for this fact is that the hottest tips of a DLA aggregate grow much faster than the deep fjords (which hardly grow at all); hence the *rate of change* of the p_i differs greatly when i is a tip perimeter site than when i is a fjord perimeter site.

Although there have been theoretical calculations of the multifractality of DLA [18–20], there had been no experimental tests of these predictions. We have recently carried out the first such tests, and found experimental confirmation of the broad outlines of the theory of multifractals [21].

There are many experimental realizations of DLA, and for the present work we will focus upon two-dimensional fractal viscous fingers since it is possible to

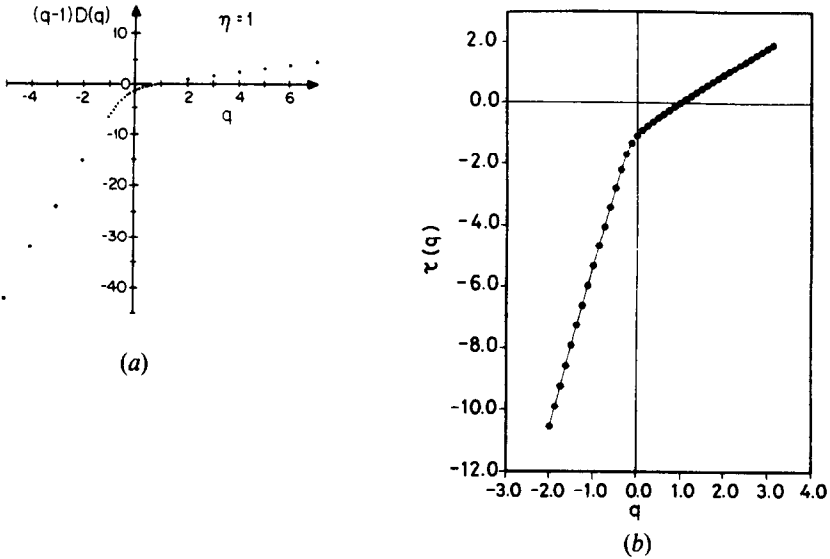


Fig. 7. Comparison of the critical exponents $\tau(q) = (q - 1)D(q)$ for (a) the theoretical and (b) 'experimental' viscous fingering patterns. In both cases, $\tau(q)$ was obtained numerically (see caption to fig. 6) (after Amitrano et al. [40] and Nittmann et al. [41]).

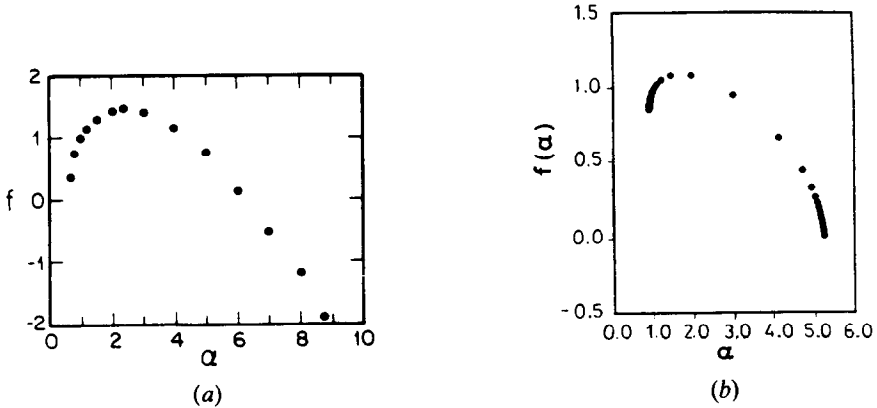


Fig. 8. Comparison between (a) theoretical and (b) 'experimental' plots of the function $f(\alpha)$ (after Amitrano et al. [40] and Nittmann et al. [41]).

study the real-time growth using a movie camera and to digitize precisely the observed time development of the DLA fractal. By subtracting two successive 'snapshots', we can obtain an accurate estimate of the appropriate normalized growth probability p_i for each perimeter site of the finger (fig. 3).

We first calculated the distribution function $n(p)$, where $n(p) dp$ is the number of perimeter sites with p_i in the range $[p_i, p_i + dp_i]$. This curve has a

long tail extending to the extremely small values of p_i for perimeter sites deep inside fjords. We found good agreement between the experimental $n(p)$ for viscous fingers (fig. 6a) and the corresponding theoretical $n(p)$ calculated for DLA (fig. 6b).

We next formed the moments $Z_q = \Sigma (p_i)^q$ which are characterized by the hierarchy of exponents τ_q defined through $Z_q = L^{-\tau_q}$, where L is a characteristic linear dimension. The experimental results (fig. 7a) show that when q is large τ_q is linear in q , but for q is small there is downward curvature in τ_q , showing that the fjords are characterized by different growth rates than the tips. It is conventional to also calculate the Legendre transform with respect to q of τ_q , $-f(\alpha) = \tau(q) - q\alpha$ where $\alpha = d\tau/dq$. Downward curvature in $\tau(q)$ corresponds to upward curvature in $-f(\alpha)$ (fig. 8a). The experimental data of figs. 7a and 8b compare favorably with the theoretical DLA model calculations shown in figs. 7b and 8b.

6. 'Dendritic fluid patterns': A variant of the fluid-mechanical model

By analogy with the Ising model and its variants, we can modify DLA/DBM to describe other fluid-mechanical phenomena. One of the most intriguing of these concerns a variation of the viscous fingering phenomenon in which there is present anisotropy. Ben-Jacob et al. [22] imposed this anisotropy by scratching a lattice of lines on their Hele-Shaw cell. They found patterns that strongly resemble snow crystals! If viscous fingers are described by DLA, can the Ben-Jacob patterns be described by DLA with imposed anisotropy?

Nittmann and Stanley [23] attempted to answer this question – specifically, they attempted to reproduce the Ben-Jacob patterns with suitably modified DLA. A scratch in a Hele-Shaw cell means that the plate spacing b is increased along certain directions, and the permeability coefficient k relating growth velocity to ∇P is proportional to $b^2 (k \propto b^2)$. Hence, Nittmann and Stanley calculated DLA patterns for the case in which there was imposed a periodic variation in k . It is significant that their simulations reproduce snow-crystal type patterns, just like the experiments. These simulations relied for their efficacy on the presence of noise reduction.

7. Noise reduction

The original DLA and DBM models are prototypes of completely chaotic systems. No discernable pattern emerges. If there is a weak anisotropy, we expect that the resulting pattern reflects this anisotropy. For example, if the simulations are carried out on a lattice, then the presence of the lattice imposes

a weak anisotropy (e.g., on a square lattice, it is more likely that particles attach to the westernmost tip if they approach from the west than from the north or south). This weak anisotropy is not visually apparent unless large clusters are grown. However, the largest DLA clusters made [8] with mass about 4 million sites, clearly display the anisotropy (fig. 9). Unfortunately, no one can afford the computer resources to make such ‘mega-DLA’ clusters each time we wish to model a new phenomenon. Noise reduction is a computational trick that seems to have the property that it speeds up the attainment of this asymptotic limit. In the absence of noise reduction, a perimeter site becomes a cluster site whenever it is chosen (e.g., whenever a random walker lands on that site).

‘Noise reduction’ means that we associate a counter with each perimeter site; each time that site is chosen, the counter increments by one. The perimeter site becomes a cluster site only after the counter reaches a pre-determined threshold value termed s [23–25]. When $s = 1$, we recover the original noisy DLA. Growth is dominated by the stochastic randomness in the arrival of random walkers. If s is very large, then growth is determined by the actual probability distribution.

For example, suppose we start with a large disc as a seed particle (instead of a single site). The growth probability at all points on the disc surface will be equal, assuming a continuum.

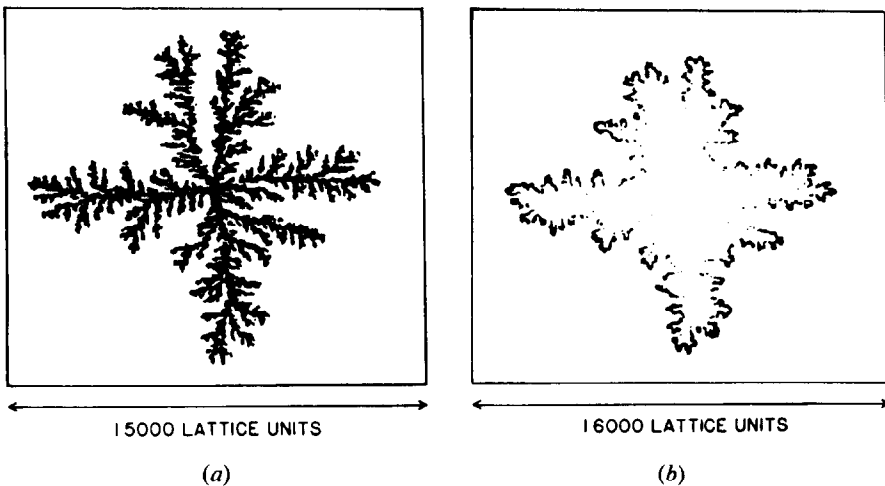


Fig. 9. (a) A huge DLA cluster with a mass of 4 million sites grown on a square lattice. (b) Shown is only the last 5% of the growth. In reality, there is structure on all scales less than the width W of the 4 arms. Moreover, W scales with cluster mass as $W \sim (1/M)^{-1/d_f}$, just in the same way as the quantity ξ_L defined in eq. (1c). The spontaneous appearance of side branches is reminiscent of experimental dendritic growth patterns such as those shown in fig. 13 (after Meakin [8]).

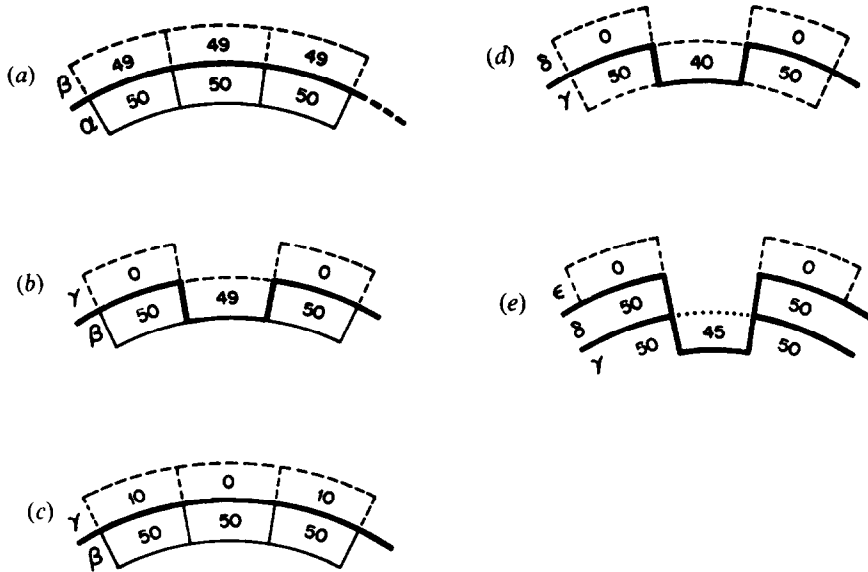


Fig. 10. Schematic illustration of the difference between an outward ('positive') and an inward ('negative') interface fluctuation. A positive fluctuation tends to be damped out rather quickly, as mass quickly attaches to the side of the extra site that is added. On the other hand, a negative fluctuation grows, in the sense that mass accumulates on both sides of the tiny notch. The notch itself has a lower and lower probability of being filled in, as it becomes the end of a longer and longer fjord. This is the underlying mechanism for the tip-splitting phenomenon when no interfacial tension is present. Part (a) shows the advancing front (row α) of a cluster with $s = 50$. The heavy line separates the cluster sites (all of which were chosen 50 times) from the perimeter sites (all of which have counters registering less than 50). In (a), no fluctuations in the counters of these three sites have occurred yet, and all three perimeter counters register 49. Part (b) shows a negative fluctuation, in which the central perimeter site is chosen slightly less frequently than the two on either side; the latter now register 50, and so they become cluster sites in row β . The perimeter site left in the notch between these two new cluster sites grows much less quickly because it is shielded by the two new cluster sites. For the sake of concreteness, let us assume it is chosen 10 times less frequently. Hence, by the time the notch site is chosen one more time, the two perimeter sites at the tips have been chosen 10 times (c). The interface is once again smooth (γ), as it was before, except that the counters on the three perimeter sites differ. After 40 new counts per counter, the situation in (d) arises. Now we have a notch whose counter lags behind by 10, instead of by 1 as in (b). Thus the original fluctuation has been amplified due to the tremendous screening of a single notch. Note that no new fluctuations were assumed: the original fluctuation of 1 in the counter number is amplified to 10 solely by electrostatic screening. This amplification of a negative 'notch fluctuation' has the effect that the tiny notch soon becomes the end of a long fjord. To see this, note that part (e) shows the same situation after 50 more counts have been added to each of the two tip counters, and hence (by the 10:1 rule) 5 new counts to the notch counter. The tip counters, therefore, become part of the cluster, but the notch counter has not yet reached 50 and remains a perimeter site. The notch has become an incipient fjord of length 2, and the potential at the end of this fjord is now exceedingly low. Indeed it is quite possible that the counter will never pass from 45 to 50 in the lifetime of the cluster. In our simulations we can see tiny notch fluctuations become the ends of long fjords, and all of the above remarks on the time-dependent dynamics of tip splitting are confirmed quantitatively (after Nittmann and Stanley [23]).

By the D'Arcy growth law, this disc should evolve in time into a larger disc. On the other hand, for ordinary DLA ($s = 1$), as soon as a random walker touches a single perimeter site on the disc, this site will become part of the cluster and the disc will lose its circular symmetry. The growth probabilities will all be re-calculated, and the perimeter sites close by the one that just grew will have higher growth probabilities. Thus, the disc with a single site added to

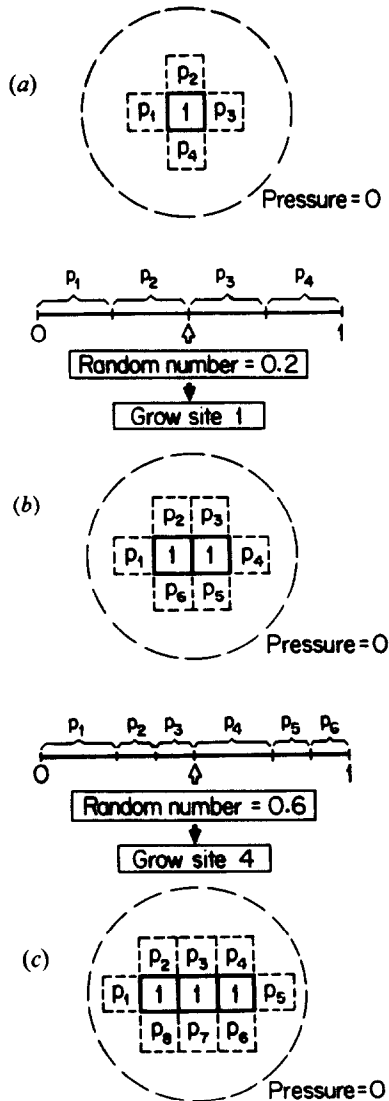


Fig. 11. Schematic illustration of the first steps in the generation of a DLA cluster by solving directly the Laplace equation on a square lattice.

it will be more likely to grow in the direction of that single site. At a later time, we will almost certainly not find a cluster with circular symmetry.

Clearly, if s is very large, then the initial growth will preserve an almost circular structure. This is because before the first site is added to the circular seed, all the perimeter sites will acquire large numbers in their counters ($s - 1, s - 2$, etc.). After the first site is added, these additional perimeter sites will be very close to the threshold for growing while the new perimeter sites that were born when the first cluster site is added will all have counters initialized at zero. A typical cluster grown in this fashion is shown in fig. 10; actually this cluster is grown on a square lattice with first and second neighbor interactions, not on a continuum. However, Meakin et al. [26] have found an almost identical pattern for the continuum case.

At first sight, there is little economy in computational speed, since one needs ' s times as many' random walkers to reach a given cluster size. Thus, to grow a cluster with merely 4000 sites with $s = 1000$ requires almost as much time as to generate a mega-DLA with 4 000 000 sites and $s = 1$. Fortunately, there is a way around this problem. Instead of using random walkers to solve the Laplace equation (to sample the growth probabilities p_i on each perimeter site), we can directly solve the Laplace equation numerically. This is the approach used when the dielectric-breakdown model was first proposed (fig. 11). Whether one calculates the growth probabilities by sending in random walkers or by solving the Laplace equation is immaterial: the difference between DLA and DBM is the boundary conditions, not the method of calculation.

The advantage of the Laplace equation approach when s is large is obvious: one need re-solve the Laplace equation only after a site is actually added to the cluster. In between adding sites, one simply chooses random numbers weighted by the growth probabilities of each perimeter site. This is a relatively rapid procedure for the computer, compared with its counterpart of sending random walkers.

8. Dendritic solid patterns: 'Snow Crystals'

Of course, real dendritic-growth patterns (such as snow crystals) do not occur in an environment with periodic fluctuations in $k(x, y)$. Rather, the *global* asymmetry of the pattern arises from the *local* asymmetry of the constituent water molecules. Can this local asymmetry give rise to global asymmetry? Buka et al. [27] replaced the Ben-Jacob experiment (isotropic fluid, anisotropic cell) by the reverse: isotropic cell but anisotropic fluid!

To accomplish this, they used a nematic liquid crystal for the high-viscosity fluid. Thus, the analog of the water molecules in a snow crystal are the

rod-shaped anisotropic molecules of a nematic. This experiment shows that the underlying anisotropy can as well be in the fluid as in the environment.

Snow crystal formation is thought to involve mainly the aggregation of tiny ice particles and droplets of supercooled water. To the extent that snow crystals grow by accreting water molecules previously in the vapor or liquid phase, the growth rate is thought to be limited by the diffusion away from the growing snow crystal of the latent heat released by these phase changes. Under conditions of small Peclet number, the diffusion equation describing the space and time dependence of the temperature field $T(\mathbf{r}, t)$ reduces to the Laplace equation. Thus a reasonable starting point is DLA, independent of whether we wish to focus on particle aggregation, heat diffusion, or both.

DLA reflects well the randomness inherent in a wide range of growth processes, including colloidal aggregation, it fails to describe dendritic solidification. While the deterministic models of snow crystals produce patterns that are much too 'symmetric', the DLA approach suffers from the opposite problem: DLA patterns are too 'noisy'. That DLA is too noisy has long been recognized as a defect of this otherwise physically appealing model. Recently, an approach has been proposed [21] that retains the 'good' features of DLA and at the same time produces patterns that resemble real (random) snow crystals.

Firstly, we introduce [21] controlled amounts of noise reduction of the same sort used previously for both DLA and for DBM. It is believed that noise-reduced DLA is in the same universality class as ordinary DLA – i.e., it has the same fractal dimension d_f , the only difference being an increase in the characteristic local length scale W . One advantage of setting $s > 1$ is that the asymptotic behavior ($M = \infty$) shows up much sooner than if $s = 1$. We do not explicitly introduce anisotropy – the only anisotropy present is the six-fold anisotropy arising from the underlying triangular lattice.

The patterns obtained [21] have the same general features for all values of s greater than about $s = 100$ – the effect of increasing s seems mainly to be that of increasing the width W of the fingers and side branches. The fjords between the 6 main branches contain much empty space. Some snow crystals have such wide 'bays', but some do not. A better model would seem to require some tunable parameter that enables the complete range of snow-crystal morphologies to be generated. We have found one such parameter, η , that has the desired effect of reducing the difference in the ratio of the growth probabilities between the tips and fjords. Specifically, we relate by the rule $p_i \propto (\nabla\phi)^\eta$ the growth probability p_i (the probability that perimeter site i is the next to grow) to the potential ϕ (e.g., ϕ may be the temperature $T(\mathbf{r})$ at point \mathbf{r} , or the probability that a tiny ice particle is at point \mathbf{r}). Our model is thus the analog for DLA of the ' η model'.

We used η to tune the balance between tip growth and fjord growth and found growth patterns that resemble better the wide range of snow-crystal morphologies than have been experimentally observed [21]. To what does the case $\eta \neq 1$ correspond? For $\eta = k$ ($k =$ positive integer), we have a model [28] in which a site grows only if it is chosen k times in succession ($k = 1$ is pure DLA). It is possible that we have a situation not altogether different from the classic n -vector model of isotropically-interacting n -dimensional classical spins: this model makes physical sense only if n is a positive integer, yet its study for other values of n has led to rich insights – particularly the cases $n = 0$ (the dilute-polymer chain limit), $n = \infty$ (the spherical model) and $n = -2$ (the mean-field limit). Similarly, the Q -state Potts model makes physical sense only if Q is an integer above 1, yet the cases $Q = 0$ (random resistor network), $Q = 1$ (percolation) and $Q = \frac{3}{2}$ (a spin-glass model) are of great interest.

The fractal dimension d_f is believed to be independent of the value of the noise reduction parameter s (s renormalizes the cluster mass). We confirmed this belief. However, we found d_f does depend on η . The most reliable estimates were obtained by first calculating estimates of d_f for a sequence of increasing cluster masses, and then extrapolating this sequence to infinite cluster mass. Our values for d_f agreed remarkably well with values we obtained by digitizing photographs of experimentally observed snow crystals. Of course this preliminary study [21] does not completely ‘solve’ the snow-crystal problem:

(i) The initial seed of a snow crystal is almost certainly hexagonal (i.e., quasi-2-dimensional), since this is the local geometry that water molecules take when they form hexagonal ice I_h . Are DBM-type considerations (small growth probability near the center of a plate-like structure) sufficient to explain why a snow crystal remains quasi-2-dimensional as it continues growing? Why does its thickness remain less than its width? It is perhaps appropriate to mention that no adequate explanation has yet been advanced for why a snow crystal remains quasi-2-dimensional throughout its growth, despite the fact that the ‘assembly plant’ is certainly 3-dimensional. Intuition on this subject stems from experience not only from critical phenomena but also from recent theoretical and experimental work on pattern formation, where it was found that even minute amounts of anisotropy are sufficient to stabilize structures of lower effective dimension.

(ii) What are the microscopic mechanisms that give rise to the feature that real snow crystals contain branches (and sidebranches) which are much more than one molecule thick? Is noise reduction relevant, or is noise reduction merely a ‘computational trick’ that allows one to see the asymptotic form of a DLA cluster using reasonable masses? (For example, on a square lattice, the same cross-like pattern for a mass of 5 000 sites seen in noise-reduced DLA

with a noise-reduction parameter of $s = 500$ is also seen in ordinary ‘noisy’ DLA ($s = 1$) provided the mass is allowed to increase to roughly 5 000 000 sites!) We know that DLA is obtained even if the incoming random walkers have a sticking probability that is less than one. Hence we anticipate that DLA might possibly describe a modest range of phenomena with structural re-arrangement. What is the actual sticking probability for newly arriving water molecules in real snow crystals? Is a value of the sticking probability less than unity sufficient to account for the fact that the arms and sidebranches of real snow crystals have macroscopic thickness?

(iii) Are those real snow crystals which possess relatively compact cores with ramified dressing on their surfaces products of different environments of assembly, or did melting and structural re-arrangement take place after formation? Can one mimic the effect of the changing environments in which a given snow crystal is actually assembled? Do these correspond to varying parameters such as η or γ in the course of the growth process? To study this effect, we generated patterns with values of η and γ that change during the growth process – e.g., we might choose $\eta \ll 1$ for an initial fraction f of the growth (thereby creating a hexagonal core), and $\eta = 1$ thereafter (thereby creating a ramified exterior portion).

(iv) Does the presence in the clouds of a wind whose direction and speed varies randomly (both in time and in space, with characteristic time scales and length scales that are microscopic) imply that the actual trajectories of water molecules and water droplets might more resemble those of some extremely ‘pathological’ path than those of a conventional DLA type random walk? We know that the random-walk trajectories of DLA correspond exactly to the present electrostatic growth model, the DBM with DLA boundary conditions. What are the trajectories in ‘real space’ corresponding to a choice of the η -parameter below unity? One can speculate that a Lévy flight with tunable fractal dimension may be related to the path of a real ice particle buffeted around in a cloud.

(v) How significant, in practice, is the role played by diffusion of latent heat away from the growing aggregate in determining the actual structure of a snow crystal? We know that this phenomenon is of paramount importance in dendritic growth of crystals from a liquid phase. How significant is the role played by the capillary length $d_0 = \gamma/L$ in vapor-phase deposition of water molecules onto a growing snow crystal? (Here L is the latent heat.) An ideal model might encompass *both* the diffusion of heat away from the snow crystal and the aggregation of particles toward the snow crystal?

(vi) Are real snow crystals sometimes fractal objects? This intriguing question has been the object of considerable discussion in recent years. Our growth patterns are fractal, for all positive values of η . We found [21] that the fractal

dimension d_f is independent of the value of the noise reduction parameter s (s seems to mainly renormalize the cluster mass), but d_f does depend on η . We also found that these values for d_f agreed well with values we obtained by digitizing the corresponding photographs of experimentally observed snow crystals (fig. 12).

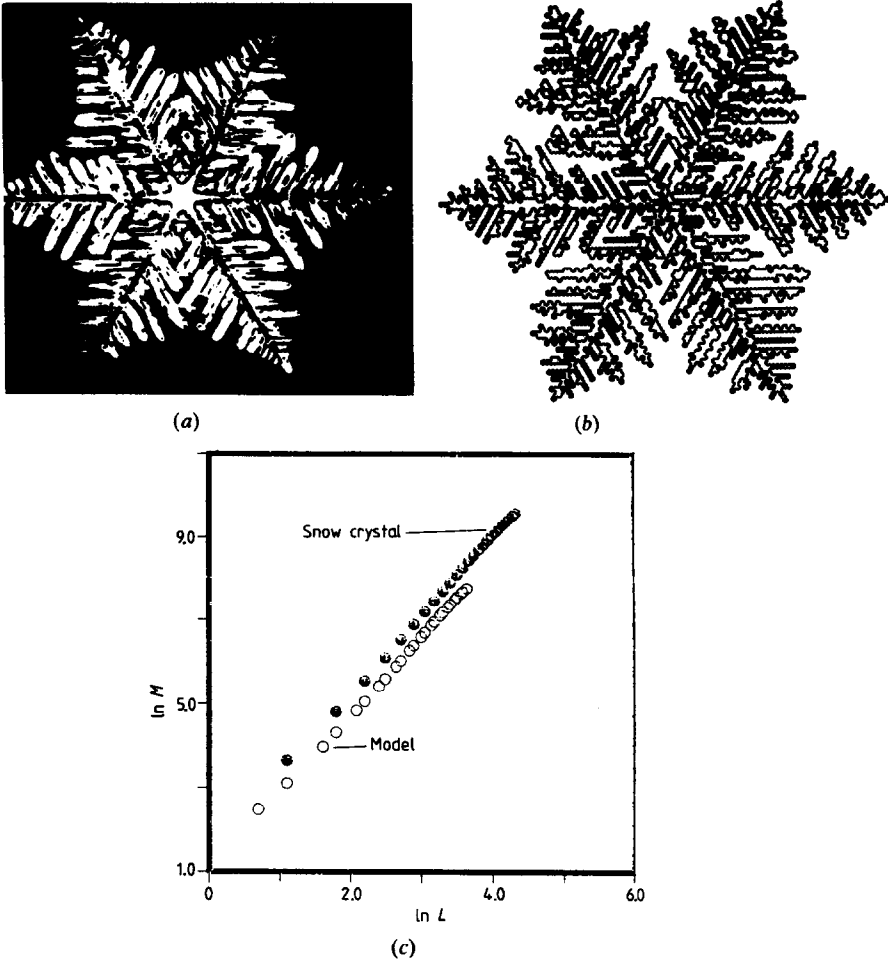


Fig. 12. (a) A typical snow crystal from the collection of 2453 photographs assembled in Bentley and Humphreys [44]. Other experimental examples may be found in Nakaya [42] and LaChapelle [43]. (b) A DLA simulation with noise-reduction parameter of $s = 200$ and non-linearity parameter $\eta = 0.5$. (c) Comparison between the fractal dimensions of (a) and (b) obtained by plotting the number of pixels inside an $L \times L$ sandbox logarithmically against L . The same slope, $d_f = 1.85 \pm 0.06$, is found for both. The experimental data extend to larger values of L , since the digitizer used to analyze the experimental photograph has 20 000 pixels while the cluster has only 4000 sites (after Nittmann and Stanley [21]).

9. Dendritic solid patterns: Growth of NH_4Br

Dendritic-crystal growth has been a field of immense recent progress, both experimentally and theoretically. In particular, Dougherty et al. [29] have recently made a detailed analysis of stroboscopic photographs, taken at 20 second intervals, of dendritic crystals of NH_4Br (fig. 13a). They have found three surprising results: (i) the sidebranches are non-periodic at any distance from the tip, with random variations in both phase and amplitude; (ii) sidebranches on opposite sides of the dendrite are essentially uncorrelated; and (iii) the rms sidebranch amplitude is an exponential function of distance from the tip, with no apparent onset threshold distance. Some of these results are apparently at variance with predictions from recent theories [30–32].

How can we understand these new experimental facts? Many existing models reflect the essential physical laws underlying the growth phenomena, but fail to

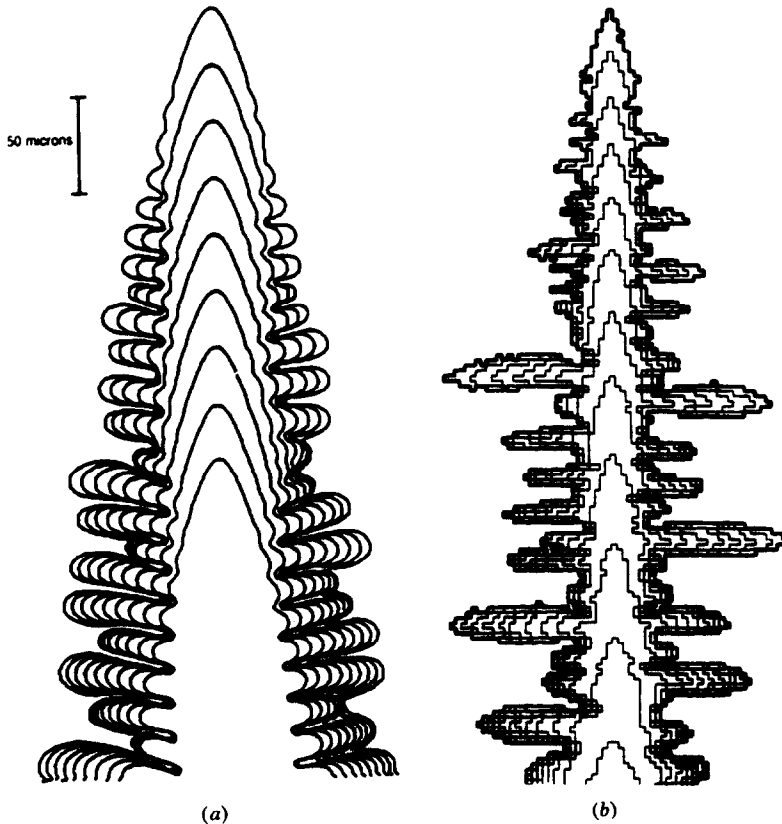


Fig. 13. (a) Experimental pattern of dendritic growth, measured for NH_4Br by Dougherty et al. [29]. (b) DLA simulation with noise-reduction parameter $s = 200$ (after Nittmann and Stanley [33]).

find a tractable mechanism to incorporate the effects of noise on the growth. Growth of a dendrite from solution is controlled by the diffusion of solute towards the growing dendrite. In the limit of small Peclet number, the diffusion equation reduces to the Laplace equation (as mentioned above). The Laplace equation for a moving interface (the growing dendrite) brings to mind the diffusion-limited aggregation model (DLA). Growth patterns produced by the various DLA simulation algorithms do *not* resemble dendritic growth patterns: DLA patterns are much too chaotic in appearance. We shall discuss here a related model [33] whose asymptotic structure does resemble the patterns found experimentally – both in broad qualitative features and in quantitative detail. The picture that emerges is one of Laplacian growth, where noise arises from the fact that there are concentration fluctuations in the vicinity of the growing dendrite (these are estimated to be roughly $\pm 10^5$ NH_4Br molecules per cubic micron).

Our starting point is the observation that minute amounts of anisotropy become magnified as the mass of a cluster increases. In fact, even the weak anisotropy of the underlying lattice structure can become so amplified that clusters of 4 000 000 particles take on a cross-like appearance (see fig. 1 of ref. [8]). A real dendrite has a mass of roughly 10^{16} particles; it is impossible to generate clusters of this size on a computer, since even clusters of size 10^6 require hundreds of hours on the fastest available computers. Fortunately, there is a computational trick – termed *noise reduction* – that speeds the convergence of the pattern toward its asymptotic ‘infinite mass’ limit. The patterns we obtained with noise-reduced DLA resemble fig. 1 of Dougherty et al. [29], reproduced in fig. 13a.

A typical result [33] for a mass of 4000 particles is shown in fig. 13b. After each 333 particles are added, a contour is drawn:

(i) It is apparent from the ‘stroboscopic’ representation of fig. 13b that the distance between successive tip positions is a decreasing function of the mass; in fact, we find that $\log x_{\text{tip}}$ is linear in $\log M$ with slope $\frac{2}{3}$. This result is consistent with the belief that $d_f = 1.5$ for DLA with anisotropy.

(ii) The tip is remarkably parabolic: Specifically, when we form $(y_c - y_0)^2$ (where y_c is the contour, and y_0 is the centerline of the dendrite) and plot this on linear graph paper as a function of $x - x_{\text{tip}}$, we obtain a straight line with an R value of 0.997.

(iii) The sidebranches are non-periodic at any distance from the tip, with random variations in both phase and amplitude. To demonstrate this, we have analyzed our simulations in exactly the same mathematical fashion as Dougherty et al. analyzed the experimental dendrite patterns.

An open theoretical question concerns the microscopic origin of the sidebranching phenomenon. One current hypothesis predicts that the sidebranch amplitude would be periodic and the two sides of the dendrite should have

correlated sidebranching. Dougherty et al. [29] noted that their experimental data are not consistent with this hypothesis, and we can make similar remarks for the present model. A second hypothesis views sidebranching as a result of the noise arising from concentration fluctuations. To test this hypothesis, Dougherty et al. [29] plot the sidebranch amplitude as a function of $x - x_{\text{tip}}$, the distance from the tip. They found that the sidebranch amplitude decreases as the distance variable $x_{\text{tip}} - x$ decreases, and shows no sign of a threshold distance below which the amplitude is zero.

Moreover, they found that close to the tip the sidebranch amplitude is roughly linear on semi-log paper. If we plot y_c , the amplitude, which should scale roughly as the square root of the area under the peak if the peak maintains its shape as a function of $x - x_{\text{tip}}$; we find exactly the same exponential growth of sidebranch amplitude with distance from the tip.

In summary, we have developed a model in which noise reduction is used to tune the effect of noise, and cubic anisotropy is introduced through the use of an underlying square lattice. The resulting patterns obtained strongly resemble the experimental patterns of Dougherty et al. both in their *qualitative* appearance and in the same degree of *quantitative* detail studied experimentally. Sidebranching arises from the fact that an approximately flat interface in the DLA problem grows trees (which resemble ‘bumps’ in the presence of noise reduction); these compete for the incoming flux of random walkers. If one tree gets ahead, it has a further advantage for the next random walker and so gets ahead still more. Thus some sidebranches grow while others do not. The characteristic spacing λ between sidebranches scales with the dendrite mass with the same exponent $\frac{2}{3}$ that characterizes the growth of dendrite length x_{tip} . Moreover, the patterns we obtain are reasonably independent of details of the simulation in that similar patterns are obtained when we vary the surface tension parameter σ over a modest range; we can also alter the boundary conditions of the model with some latitude and even allow for non-linearity in the growth process ($\eta \neq 1$).

The significance of the present findings is that the essential physics embodied in the DLA model – previously used to describe fluid–fluid displacement phenomena (‘viscous fingering’) – seems sufficient to describe the highly uncorrelated (almost random) dendritic growth patterns recently discovered from the experiments and quantitative analysis of Dougherty et al.

10. Summary

We have argued that it is worth exploring all the consequences of a straightforward physical model. Our optimism is based on the success of the

Ising model and percolation in the past. We must be mindful that substantial variants of the original model may be called for. In our case, e.g., anisotropy must be introduced or else the pattern bears absolutely no resemblance to dendritic growth. Also, noise reduction must be introduced or else the computer time becomes prohibitive.

This modest work perhaps raises more questions than it answers, but it, nonetheless, might stimulate further investigation of the basic physics of random systems that must be better understood in order to explain experimentally observed non-symmetric dendritic-growth patterns and fluid-mechanics patterns. The reader interested in more details than provided here may consult recent reviews on the subject [34–39].

Acknowledgements

I'd like to thank the Organizing Committee for inviting me. The results I report here are largely due to interactions with A. Coniglio, G. Daccord, P. Meakin, E. Touboul, T.A. Witten and, most especially, J. Nittmann.

References

- [1] W. Lenz, *Phys. Z.* 21 (1920) 613.
- [2] E. Ising, *Ann. Physik* 31 (1925) 253.
- [3] J. Kertész, D. Stauffer and A. Coniglio, *Ann. Isr. Phys. Soc. (Israel)*, Adler, Deutscher and Zallen, eds. (1983) 121.
- [4] A. Geiger and H.E. Stanley, *Phys. Rev. Lett.* 49 (1982) 1895.
- [5] E.T. Gawłinski and H.E. Stanley, *J. Phys. A.* 14 (1981) L291.
- [6] A. Geiger and H.E. Stanley, *Phys. Rev. Lett.* 49 (1982) 1749.
- [7] R. Ball, *Physica A* 140 (1986) 62.
- [8] P. Meakin, in: *Phase Transitions and Critical Phenomena*, C. Domb and J. Lebowitz, eds. (Academic Press, New York, 1988), vol. 12 p. 335.
- [9] S. Chandrasekhar, *Rev. Mod. Phys.* 15 (1943) 1.
- [10] L. Niemeyer, L. Pietronero and H.J. Weismann, *Phys. Rev. Lett.* 52 (1984) 1033.
- [11] T.A. Witten and L.M. Sander, *Phys. Rev. Lett.* 47 (1981) 1400.
- [12] J. Nittmann, G. Daccord and H.E. Stanley, *Nature* 314 (1985) 141.
- [13] G. Daccord, J. Nittmann and H.E. Stanley, *Phys. Rev. Lett.* 56 (1986) 336.
- [14] K.J. Måløy, J. Feder and T. Jøssang, *Phys. Rev. Lett.* 55 (1985) 2688.
U. Oxaal, M. Murat, F. Boger, A. Aharony, J. Feder and T. Jøssang, *Nature* 329 (1987) 32.
- [15] J.D. Chen and D. Wilkinson, *Phys. Rev. Lett.* 55 (1985) 1892.
J.D. Chen, *J. Fluid Mech.* 201 (1989) 223.
- [16] H.E. Stanley, *J. Phys. A* 10 (1977) L211.
- [17] A. Coniglio, *J. Phys. A* 15 (1982) 3829.
- [18] P. Meakin, H.E. Stanley, A. Coniglio and T.A. Witten, *Phys. Rev. A* 32 (1985) 2364.
- [19] P. Meakin, A. Coniglio, H.E. Stanley and T.A. Witten, *Phys. Rev. A* 34 (1986) 3325.
- [20] T.C. Halsey, P. Meakin and I. Procaccia, *Phys. Rev. Lett.* 56 (1986) 854.

- [21] J. Nittmann and H.E. Stanley, *J. Phys. A* 20 (1987) L1185.
- [22] E. Ben-Jacob, R. Godbey, N.D. Goldenfield, J. Koplik, H. Levine, T. Mueller and L.M. Sander, *Phys. Rev. Lett.* 55 (1985) 1315.
- [23] J. Nittmann and H.E. Stanley, *Nature* 321 (1986) 663.
- [24] C. Tang, *Phys. Rev. A* 31 (1985) 1977.
- [25] J. Kertész and T. Vicsek, *J. Phys. A* 19 (1986) L257.
- [26] P. Meakin, F. Family and T. Vicsek, *J. Colloid Interface Sci.* 177 (1987) 394.
- [27] A. Buka, J. Kertész and T. Vicsek, *Nature* 323 (1986) 424.
- [28] P. Meakin, *J. Theor. Biol.* 118 (1986) 101.
- [29] A. Dougherty, P.D. Kaplan and J.P. Gollub, *Phys. Rev. Lett.* 58 (1987) 1652.
- [30] Y. Saito, G. Goldbeck-Wood and H. Müller-Krumbhaar, *Phys. Rev. Lett.* 58 (1987) 1541.
- [31] E. Ben-Jacob, N. Goldenfield, B.G. Kotliar and J.S. Langer, *Phys. Rev. Lett.* 53 (1984) 2110.
- [32] D. Kessler, J. Koplik and H. Levine, *Phys. Rev. A* 30 (1984) 3161.
- [33] J. Nittmann and H.E. Stanley, *J. Phys. A* 20 (1987) L981.
- [34] H.E. Stanley and N. Ostrowsky (eds.), *On Growth and Form: Fractal and Non-Fractal Patterns in Physics* (Martinus Nijhoff, Dordrecht, 1986).
- [35] L. Pietronero and E. Tosatti (eds.), *Fractals in Physics* (North Holland, Amsterdam, 1986).
- [36] H.E. Stanley and P. Meakin, *Nature* 335 (1988) 405.
- [37] J. Feder, *Fractals* (Pergamon, Oxford, 1988).
- [38] H.E. Stanley and N. Ostrowsky (eds.) *Random Fluctuations and Pattern Growth: Experiments and Models* (Kluwer Academic Publishers, Dordrecht, 1988).
- [39] T. Vicsek, *Fractal Growth Phenomena* (World Scientific, Singapore, 1989).
- [40] C. Amitrano, A. Coniglio and F. DiLiberto, *Phys. Rev. Lett.* 57 (1986) 1016.
- [41] J. Nittmann, H.E. Stanley, E. Touboul and G. Daccord, *Phys. Rev. Lett.* 58 (1987) 619.
- [42] U. Nakaya, *Snow Crystals* (Harvard Univ. Press, Cambridge, 1954).
- [43] E.R. LaChapelle, *Field Guide to Snow Crystals* (Univ. Washington Press, Seattle, 1969).
- [44] W.A. Bentley and W.J. Humphreys, *Snow Crystals* (Dover, New York, 1962).